Chapter 1

Thermonuclear Reactors and Solar Neutrinos

> *"A plasma must be hot enough, dense enough, and confined long enough: that is the content of the Lawson criterion."*
>
> J. D. Lawson (1957)

Lectures 25–26 developed fusion energetics, Coulomb tunneling, the thermal rate $\langle \sigma v \rangle$, and the Gamow peak. Those tools explain *why* fusion releases energy and *how fast* it proceeds in a Maxwellian gas. This chapter turns to the two settings in which that rate must actually earn its keep: laboratory thermonuclear reactors, which must confine a multi-keV plasma without melting the vessel, and the solar core, whose neutrinos provide a clean, prompt test of the proton–proton chain [6, 1, 14, 36, 32].

1.1 The reactor problem

A fusion plasma stores thermal energy in ions and electrons, deposits fusion energy through charged reaction products, and simultaneously loses energy by radiation (chiefly electron–ion bremsstrahlung) and by particle and heat transport to the wall. Net thermonuclear gain therefore requires that the fusion energy deposited while the plasma remains hot exceed the energy that was invested to heat it, and, in a practical device, exceed continuing losses as well. That comparison is the content of Lawson's criterion [1, 6].

In symbols the fusion power density is

$$p_{\mathrm{fus}} = \frac{n_X n_Y}{1 + \delta_{XY}} \langle \sigma v \rangle \, Q_{\mathrm{dep}}, \tag{1.1}$$

with Q_{dep} the energy retained in charged products. Neutrons and neutrinos leave the plasma and do not heat it; in a D + T machine the 14 MeV neutron must be caught in a blanket, while only the 3.5 MeV α heats the fuel on the spot [6, 1]. The engineering problem is to arrange density, temperature, and confinement time so that $\int p_{\mathrm{fus}} \, \mathrm{d}t$ beats heating plus losses for a useful volume and duty cycle – either by magnetic bottles (tokamaks, stellarators) or by crushing a solid pellet so violently that inertia itself holds the fuel together for nanoseconds [6, 1].

1.2 Lawson criterion: every step

1.2.1 Setup (identical-species estimate)

Start from the identical-species D + D bookkeeping [1]. Let the ion density of each fuel species be $n/2$ in a plasma of total ion density n, with equal electron density $n_e = n$ for quasineutrality. The reaction rate density is

$$r = \left(\frac{n}{2}\right)\left(\frac{n}{2}\right)\langle\sigma v\rangle = \frac{n^2}{4}\langle\sigma v\rangle. \tag{1.2}$$

If the plasma is held at the required temperature and density for a time τ, the fusion energy deposited per unit volume is

$$E_f = r\,Q\,\tau = \frac{n^2}{4}\langle\sigma v\rangle\,Q\,\tau, \tag{1.3}$$

where Q is the energy that remains available to the plasma per fusion (the energy retained in the plasma per fusion). The same algebra with unequal densities n_1, n_2 replaces $n^2/4$ by $n_1 n_2$ (or $n_1 n_2/2$ for identical particles counted once), which is how the D + T case is written in the literature [1, 6].

1.2.2 Thermal energy to be recovered

Ions and electrons each contribute $\frac{3}{2} n k_B T$ per unit volume when $n_e = n$, so the thermal investment per unit volume is

$$E_{\text{th}} = 3\,n\,k_B T. \tag{1.4}$$

Above the bremsstrahlung "crossing" temperature one may first ignore radiation and ask only that fusion repay the heating bill; at lower T, or for fuels with smaller $\langle\sigma v\rangle$, radiation must be kept explicitly and tightens the required $n\tau$ [1, 6].

1.2.3 The inequality

Demand $E_f > E_{\text{th}}$:

$$\frac{n^2}{4}\langle\sigma v\rangle\,Q\,\tau > 3\,n\,k_B T. \tag{1.5}$$

Cancel one power of n (assuming $n > 0$) and rearrange:

$$\boxed{n\tau > \frac{12\,k_B T}{\langle\sigma v\rangle\,Q}}. \tag{1.6}$$

This is the **Lawson criterion**; $n\tau$ is the Lawson parameter [1, 6, 14]. The right-hand side depends on temperature through both the explicit T and the strongly temperature dependent reactivity $\langle\sigma v\rangle(T)$ from Lecture 26. Raising $\langle\sigma v\rangle$ at fixed T therefore lowers the required product: that is why D + T is the first fuel of every practical design discussion.

An order-of-magnitude estimate at $k_B T = 10\,\text{keV}$ for D + T gives $n\tau \gtrsim 10^{20}\,\text{s}\,\text{m}^{-3}$. For D + D the same temperature is already too cool because bremsstrahlung dominates; operating near $k_B T = 100\,\text{keV}$ pushes the Lawson product up by roughly two orders of magnitude [6]. Thus a D + D reactor is not merely "harder by Q": it demands a hotter plasma and a larger $n\tau$ before radiation allows net gain.

1.2.4 Triple product

Multiplying (1.6) by T defines the triple product $n\tau T$. Over the decade $T \sim 10$–$20\,\mathrm{keV}$ where $\mathrm{D+T}$ is most reactive, $\langle \sigma v \rangle$ scales roughly as T^2, so the right-hand side becomes nearly constant. For $\mathrm{D+T}$ the practical ignition ballpark is

$$n\,\tau\,T \gtrsim 3 \times 10^{21}\,\mathrm{m^{-3}\,keV\,s} \tag{1.7}$$

[1]. Modern campaigns therefore quote $n\tau T$ rather than $n\tau$ alone, because a device that is hotter but less well confined can still sit above the ridge if the product compensates.

1.2.5 Gain Q and ignition

Facility **gain** Q_{eng} is the ratio of fusion energy out to energy invested in the plasma (and, more broadly, in the plant). $Q_{\mathrm{eng}} \sim 1$ is scientific breakeven; a power plant needs much higher values once conversion efficiency and recirculating power are counted. **Ignition** means charged fusion products alone maintain the plasma temperature: external heating can be switched off and $Q_{\mathrm{eng}} \to \infty$ for the plasma itself [1, 6]. Because the $\mathrm{D+T}$ neutron does not heat the fuel, lithium-bearing blankets both convert neutron energy to heat for electricity and breed tritium through $n + {}^6\mathrm{Li} \to \alpha + t$ (and related channels) [1, 2, 32].

Order-of-magnitude parameters for the three confinement philosophies appear in Table 1.1: magnetic bottles buy seconds at $n \sim 10^{20}\,\mathrm{m^{-3}}$; inertial capsules buy nanoseconds at $n \sim 10^{31}\,\mathrm{m^{-3}}$; the Sun buys geological times at solar-core density [14, 6].

Table 1.1: Order-of-magnitude confinement parameters [14].

Scheme	$n\,(\mathrm{m^{-3}})$	$\tau\,(\mathrm{s})$	$T\,(\mathrm{keV})$
Tokamak (ITER-class)	10^{20}	~ 1	10–20
Inertial (laser capsule)	10^{31}	10^{-11}	~ 10
Solar core (gravity)	$\sim 10^{31}$	10^{17}	~ 1

1.3 Magnetic confinement

A multi-keV plasma melts any material wall and cools on contact. **Magnetic confinement** uses the Lorentz force $q\,\boldsymbol{v} \times \boldsymbol{B}$ so that charged particles spiral about field lines and, if the field geometry is clever enough, never hit the wall [6, 1, 2]. Figures 1.1 and 1.2 show a real magnetic-confinement machine – the Joint European Torus (JET) – as photograph and cutaway; Fig. 1.3 shows the much larger ITER tokamak under construction as an international burning-plasma experiment.

1.3.1 Motion in a magnetic field

Perpendicular to $\boldsymbol{B}$, a particle of mass m, charge q, and speed $v_\perp$ gyrates with cyclotron radius

$$\rho_c = \frac{m v_\perp}{|q| B}. \tag{1.8}$$

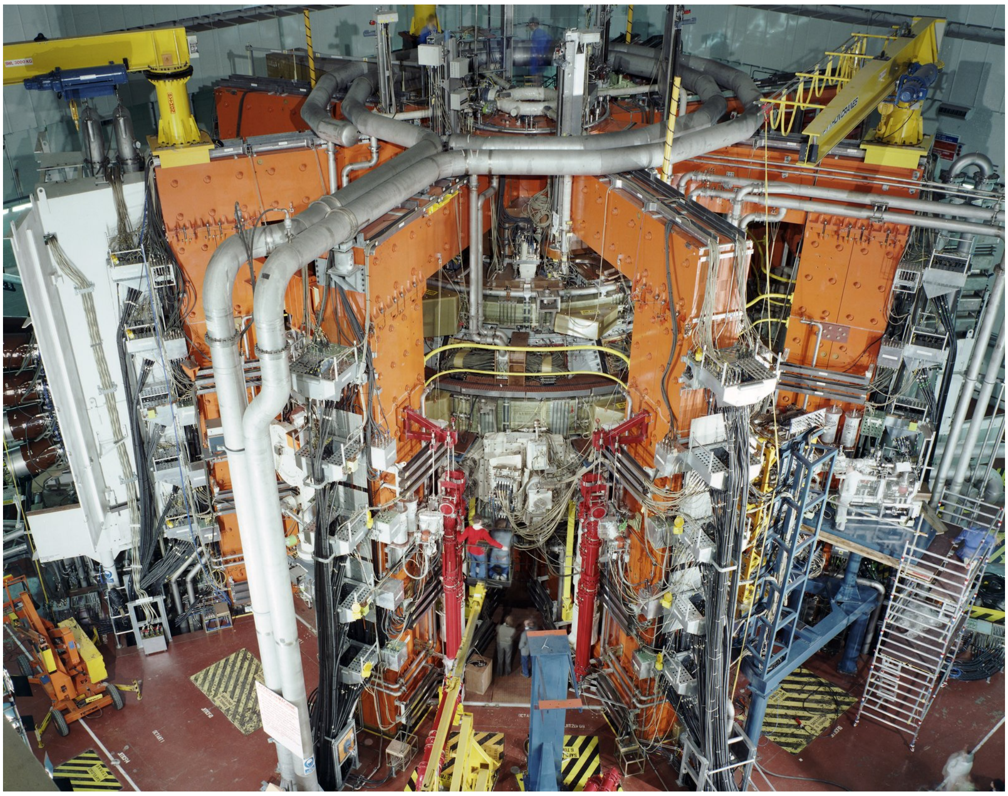

Figure 1.1: The Joint European Torus (JET) during magnetic fusion operation (1991). JET has been the leading European D–T capable tokamak and a principal pathfinder for ITER. Image: EUROfusion / EFDA (Wikimedia Commons), CC BY-SA 3.0.

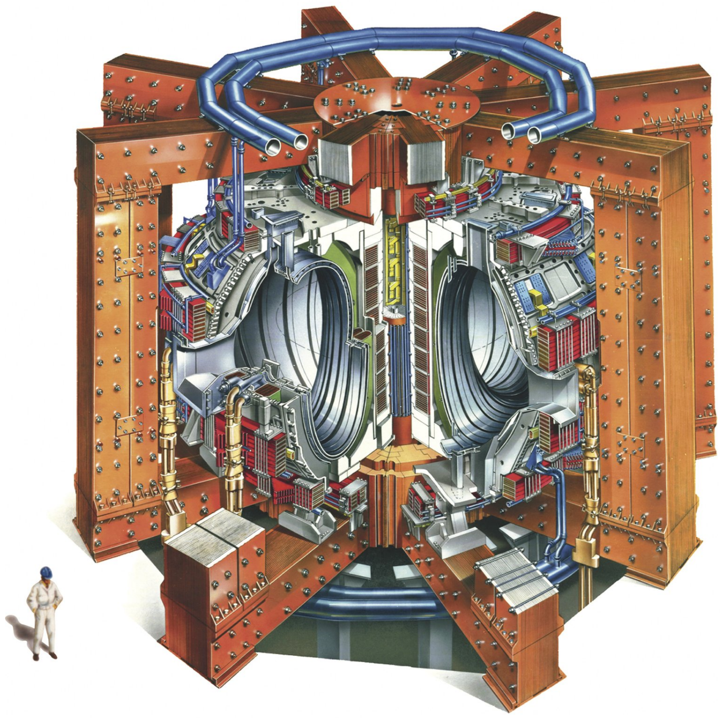

Figure 1.2: Cutaway drawing of JET (1980 design), showing the toroidal vacuum vessel, magnetic coils, and diagnostic ports around the plasma chamber. Image: EUROfusion (Wikimedia Commons), CC BY 4.0.

Parallel motion is free. A uniform field therefore confines only two spatial directions: particles stream out the ends of a finite solenoid. Textbooks give two remedies: bend the field into a **torus**, closing the field lines, or raise B at the ends of a linear bottle to form a **magnetic mirror** that reflects particles with sufficiently large magnetic moment [6, 1].

1.3.2 Why a pure torus still fails

Closing the field into a torus is not enough by itself. In a purely toroidal field, $|B|$ is stronger on the inside of the doughnut (smaller major radius R). Gradient and curvature drifts then send ions and electrons in opposite vertical directions. The resulting charge separation builds an electric field; the subsequent $\boldsymbol{E} \times \boldsymbol{B}$ drift drives the whole plasma into the outer wall [6, 14]. A particle spiralling in a real toroidal winding sees a weaker field at larger major radius, so the spiral opens toward the outer wall unless a poloidal field component is added [6].

1.3.3 Tokamak: toroidal plus poloidal fields

The tokamak cures the drift by twisting the field lines. External coils produce a strong **toroidal** field $\boldsymbol{B}_t$. A large toroidal **plasma current** (often mega-amperes) produces a **poloidal** field $\boldsymbol{B}_p$. The resultant $\boldsymbol{B} = \boldsymbol{B}_t + \boldsymbol{B}_p$ has helical field lines: particles streaming along $\boldsymbol{B}$ sample both the inner and outer major-radius regions and average away the vertical drift [6, 1, 2, 32]. Toroidal coils plus an axial plasma current produce a helical field with closed orbits [6].

In practice the plasma current is induced, transformer-style, by ohmic heating coils; that current also heats the plasma resistively until the conductivity rises and auxiliary heating (neutral beams, radio-frequency waves) takes over [6, 1]. Stellarators produce the rotational transform with shaped external coils and little net plasma current, trading coil complexity for reduced current-driven instability [1, 14]. ITER (Fig. 1.3) is designed as the step from present-day $Q_{\text{eng}} \sim$ few machines toward a sustained burning plasma with $Q_{\text{eng}} \gtrsim 10$, using superconducting magnets, remote-handling blankets, and tritium breeding technology that JET could only prototype.

1.4 Inertial confinement

Inertial confinement never builds a magnetic bottle. A millimetre-scale cryogenic D–T capsule is irradiated nearly isotropically by intense laser (or heavy-ion) beams. Ablation of the outer shell drives an implosion: the fuel is compressed and heated until a hotspot satisfies Lawson for a time set by hydrodynamic disassembly ($\tau \sim 10^{-11}$–10^{-9} s) [6, 1, 32]. Because τ is tiny, n must be enormous ($\sim 10^{31}\,\mathrm{m}^{-3}$; see Table 1.1), so that the product $n\tau$ still clears the Lawson ridge of Table 1.1. Drive asymmetry and Rayleigh–Taylor growth of the shell are the classic failure modes: any seed perturbation that grows during acceleration can spoil the hotspot before burn begins [6, 1].

Figure 1.5 shows the NIF target chamber – a real inertial device whose scale is set by laser ports, debris shields, and diagnostics rather than by toroidal magnets. Confine by inertia, not by $\boldsymbol{B}$, and pay for the short τ with extreme density [6].

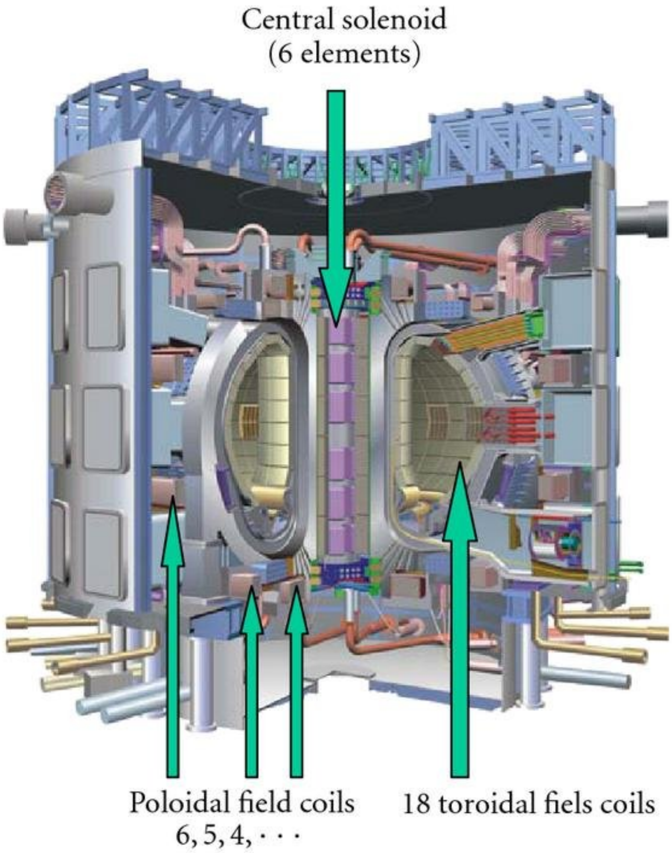

Figure 1.3: Sectional view of the ITER tokamak reactor, showing the vacuum vessel, blanket modules, and superconducting magnet systems that will confine a burning D–T plasma. Image: from Miri *et al.*, *Modelling and Simulation in Engineering* (2008), Wikimedia Commons, CC BY 4.0.

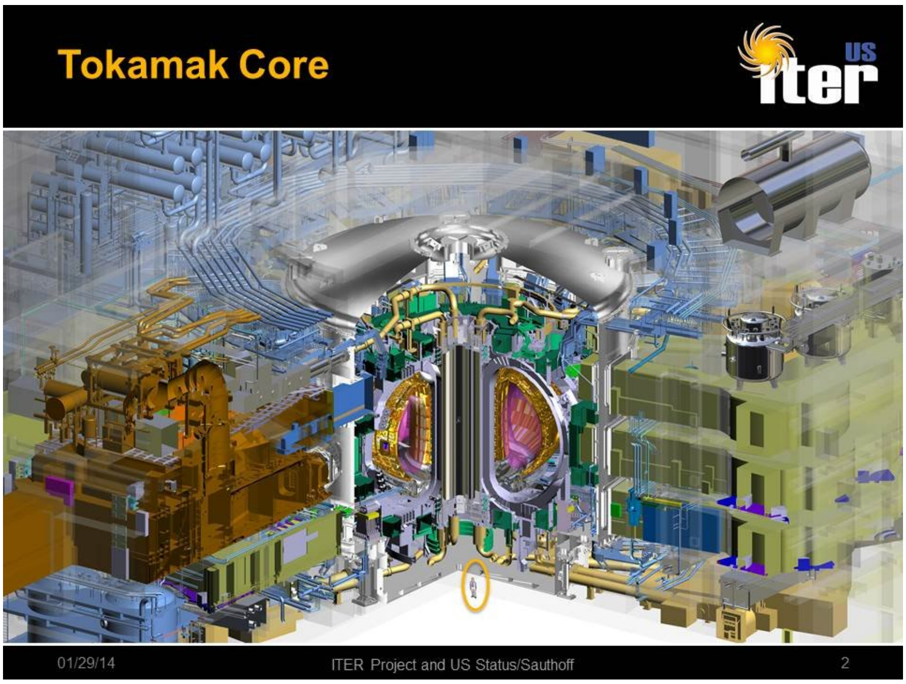

Figure 1.4: Interior of a tokamak-style fusion core mock-up / experiment (Oak Ridge National Laboratory photograph), illustrating the scale of the vacuum vessel relative to a person. Image: ORNL / Flickr via Wikimedia Commons, CC BY 2.0.

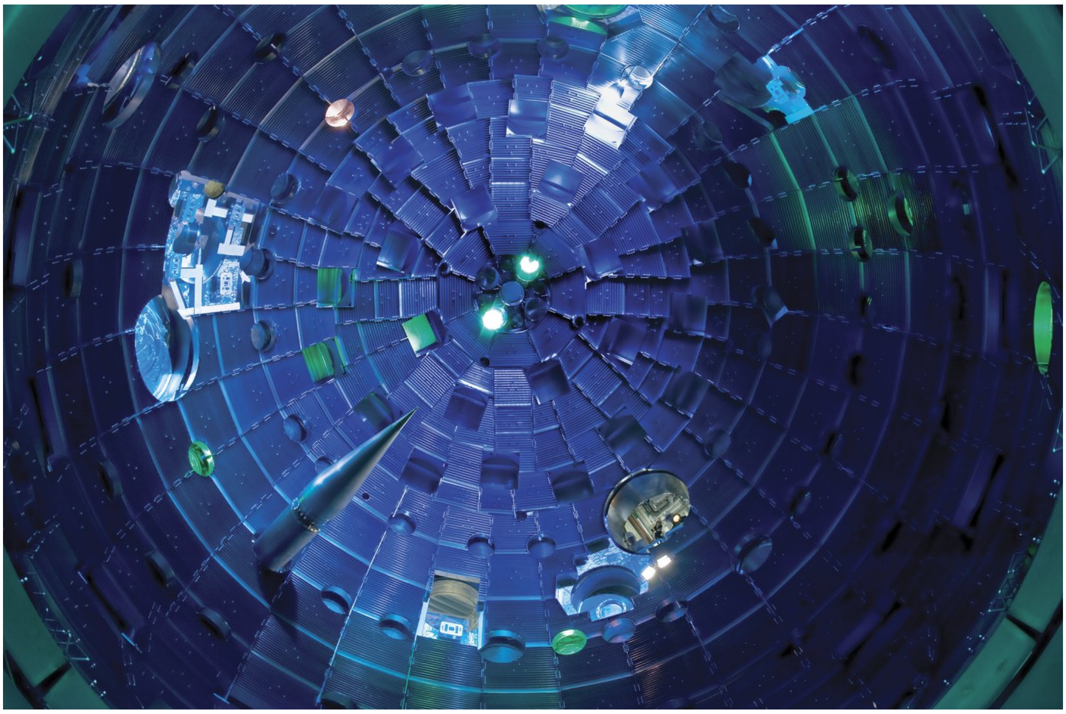

Figure 1.5: Target chamber of the National Ignition Facility (NIF) at Lawrence Livermore National Laboratory. Up to 192 ultraviolet laser beams enter the chamber to irradiate a cryogenic D–T capsule in an inertial-confinement geometry. Image: LLNL / L. Seaver (Wikimedia Commons), CC BY-SA 3.0.

1.5 Stellar hydrogen burning

Stars solve confinement with gravity. The solar core sits near $T \sim 1.3\,\mathrm{keV}$ ($\sim 1.5 \times 10^7\,\mathrm{K}$): cooler than a tokamak, but denser and longer-lived by many orders of magnitude, so the Gamow peak of the weak $p + p$ reaction still powers the Sun [14, 36, 6, 1].

1.5.1 Net stoichiometry

Every hydrogen-burning path obeys

$$4\,{}^1\mathrm{H} \;\rightarrow\; {}^4\mathrm{He} + 2e^+ + 2\nu_e, \tag{1.9}$$

with nuclear $Q \approx 26.7\,\mathrm{MeV}$ from atomic masses [1, 36]. Neutrinos escape, so the stellar heat deposit is $Q_{\mathrm{heat}} = Q - \sum \langle E_\nu \rangle$ [36, 1]. Photons random-walk for $\sim 10^4$–10^6 years to the photosphere; neutrinos free-stream from the core in minutes and therefore report on nuclear burning *now*. The light we see comes from the surface, while solar neutrinos come directly from the core reactions [6, 32].

1.5.2 The *pp* chain, branch by branch

Figure 1.6 shows the solar networks as drawn for open use. The dominant *pp* path proceeds as follows [1]:

(i) **Initiation (weak).** $p + p \rightarrow d + e^+ + \nu_e$. The cross section is of weak order and cannot be measured by colliding beams in the laboratory; the rate is inferred from theory calibrated to solar models and to the few available laboratory constraints on related reactions [14, 36].

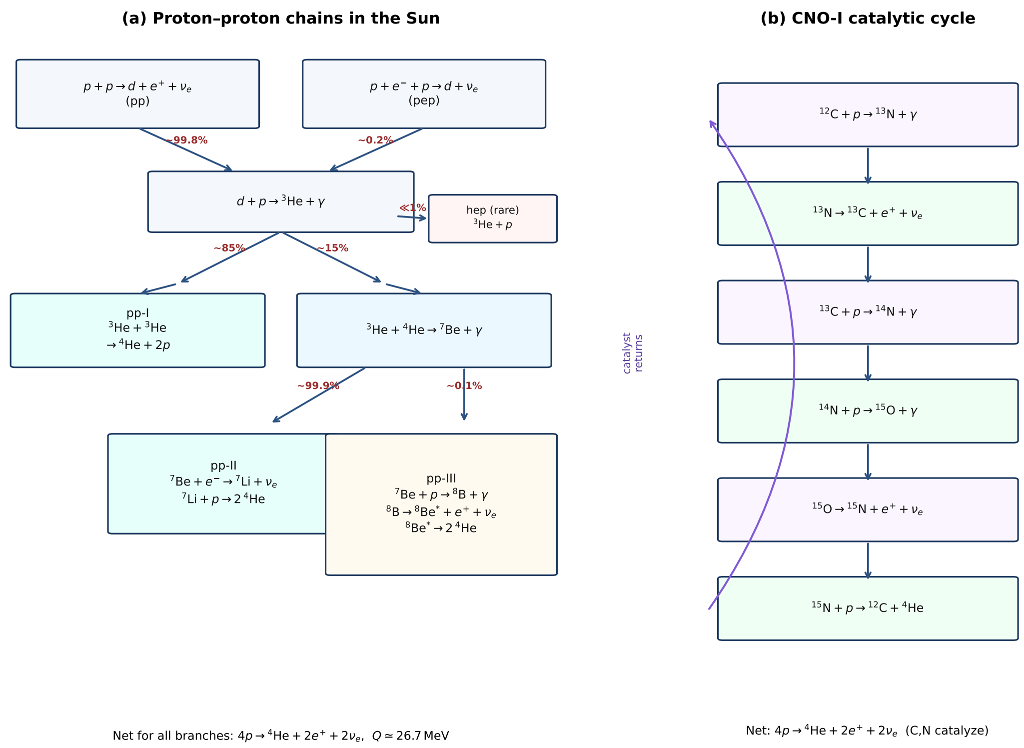

Figure 1.6: Solar hydrogen burning. (a) Proton–proton chains with approximate solar branching fractions: pp-I dominates; pp-II/III proceed through ^{7}Be; pep and hep are rare. (b) CNO-I catalytic cycle returning ^{12}C. Every branch has the same net stoichiometry $4p \to {}^4\mathrm{He} + 2e^+ + 2\nu_e$ with $Q \simeq 26.7\,\mathrm{MeV}$ [1, 36, 6].

(ii) **Deuterium burning.** $d + p \to {}^3\mathrm{He} + \gamma$ ($Q \approx 5.5\,\mathrm{MeV}$) is strong/electromagnetic and essentially instantaneous on stellar timescales.

(iii) **Termination.** *pp*-I: ${}^3\mathrm{He} + {}^3\mathrm{He} \to \alpha + 2p$ ($Q = 12.86\,\mathrm{MeV}$) [1]. *pp*-II/III: ${}^3\mathrm{He} + \alpha \to {}^7\mathrm{Be}$, then electron capture (*pp*-II) or *p*-capture to ^{8}B (*pp*-III). ^{8}B beta decay yields a hard neutrino continuum crucial for water Cherenkov detectors [6, 1, 36].

The net of four protons to one α, with two weak branches, releases $Q = 26.7\,\mathrm{MeV}$; only a small fraction leaves as neutrino kinetic energy [1].

1.5.3 CNO catalysis

When CNO nuclei are present, the CNO-I loop

$$
\begin{aligned}
{}^{12}\mathrm{C}(p,\gamma)^{13}\mathrm{N}(\beta^+\nu_e)^{13}\mathrm{C}(p,\gamma)^{14}\mathrm{N} \\
(p,\gamma)^{15}\mathrm{O}(\beta^+\nu_e)^{15}\mathrm{N}(p,\alpha)^{12}\mathrm{C}
\end{aligned}
$$

again converts four protons to one alpha. In the Sun it contributes only a few percent of the luminosity because of the larger Coulomb barriers; it dominates in hotter massive stars [1, 14, 36]. Solar neutrinos from CNO β^+ decays are therefore a small but increasingly measured correction on top of the *pp* flux hierarchy.

1.6 Solar neutrino experiments

1.6.1 Homestake chlorine detector

The most extensive early solar-neutrino programme was started in the late 1960s by Raymond Davis, Jr., in the Homestake Mine in South Dakota [1, 6]. A $380\,\mathrm{m}^3$ tank of perchloroethylene C_2Cl_4 was placed 1478 m (4850 ft) underground to suppress cosmic-ray backgrounds (Figs. 1.7–1.8). Natural chlorine is about 24% ^{37}Cl. Electron neutrinos capture via

$$\nu_e + {}^{37}\mathrm{Cl} \to e^- + {}^{37}\mathrm{Ar}, \qquad E_{\mathrm{th}} = 0.814\,\mathrm{MeV}. \tag{1.10}$$

Inspection of the solar spectrum shows that Homestake is dominated by ^{8}B neutrinos, with smaller contributions from pep and ^{7}Be; the *pp* continuum lies almost entirely below threshold [1]. The daughter ^{37}Ar returns to ^{37}Cl by electron capture (half-life 35 d; mean life of order fifty days); argon is swept chemically from the tank on a one–two month cycle and counted via characteristic Auger electrons in a small proportional counter [1, 6].

Figure 1.7: Homestake Mine solar-neutrino detector: the large perchloroethylene tank of the Brookhaven / Davis chlorine experiment, photographed underground. Public-domain U.S. Department of Energy photograph (Wikimedia Commons, HD.6B.411).

The expectation is roughly one argon atom produced per day in Davis's tank, yet the observed rate was only about one-third of the Standard Solar Model prediction [6]. After approximately thirty years of running, the Homestake result is 2.55 ± 0.25 SNU against a predicted 8.0 ± 1.0 SNU (one SNU $= 10^{-36}$ captures per target nucleus per second), for a detector mass of 1.3×10^5 kg of ^{37}Cl nuclei [1]. That persistent deficit is the classic **solar neutrino problem**.

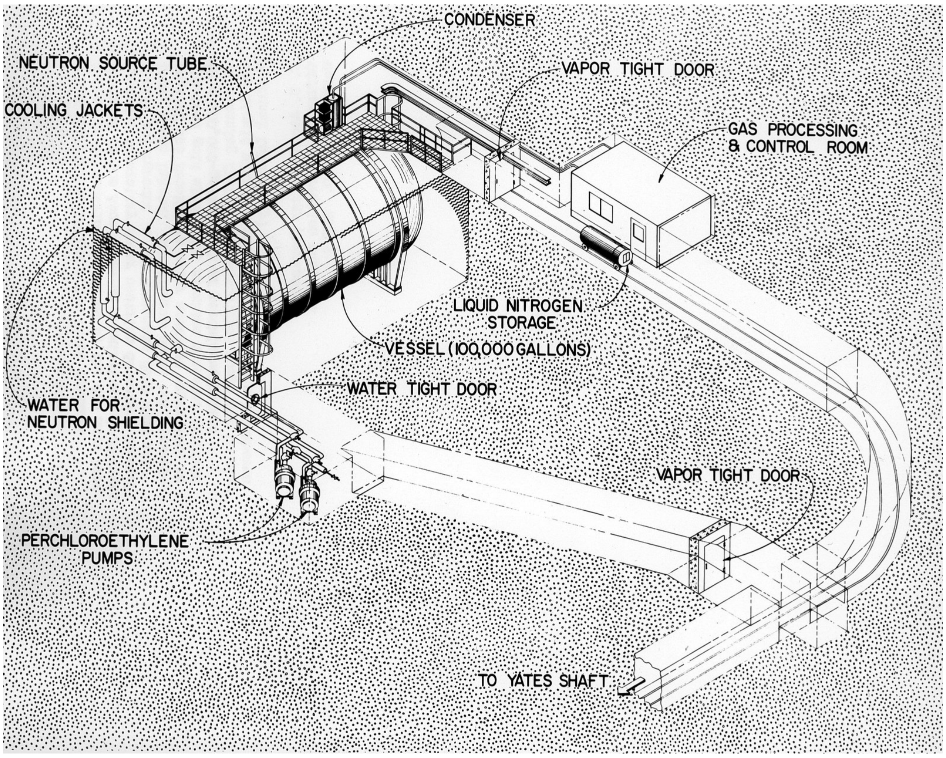

Figure 1.8: Contemporary diagram of the Brookhaven National Laboratory solar neutrino detector in the Homestake Mine (c. 1972), showing the tank, helium-sweep plumbing, and argon extraction system used to count ^{37}Ar. Public-domain U.S. Atomic Energy Commission / DOE diagram (Wikimedia Commons).

1.6.2 Gallium and water Cherenkov

Gallium experiments (SAGE in Russia; GALLEX and later GNO near Rome) use

$$\nu_e + {}^{71}\mathrm{Ga} \to e^- + {}^{71}\mathrm{Ge}, \tag{1.11}$$

with threshold $\approx 0.23\,\mathrm{MeV}$, so *pp* neutrinos are admitted. Extracted ^{71}Ge decays back to ^{71}Ga with a lifetime of 16.5 d; periodic chemical extraction again provides a radiochemical rate. SAGE and GALLEX/GNO agree with each other but still fall below Standard Solar Model predictions, typically near half the expected rate [1].

Kamiokande and Super-Kamiokande detect νe elastic scattering by Cherenkov light in ultrapure water. The recoil electron points approximately back to the Sun, confirming the solar origin, but the channel is still dominated by high-energy ^{8}B neutrinos [1, 14, 2]. Figure 1.9 shows the interior of Super-Kamiokande: thousands of photomultiplier tubes viewing a vast water volume – the same detection principle used for solar νe scattering, atmospheric neutrinos, and supernova bursts.

1.6.3 Resolution: flavour oscillation and MSW

Radiochemical detectors count ν_e only. The Sudbury Neutrino Observatory (SNO) in Ontario used 1000 t of heavy water in a 12 m acrylic vessel, beginning physics data in 1999 [1]. On

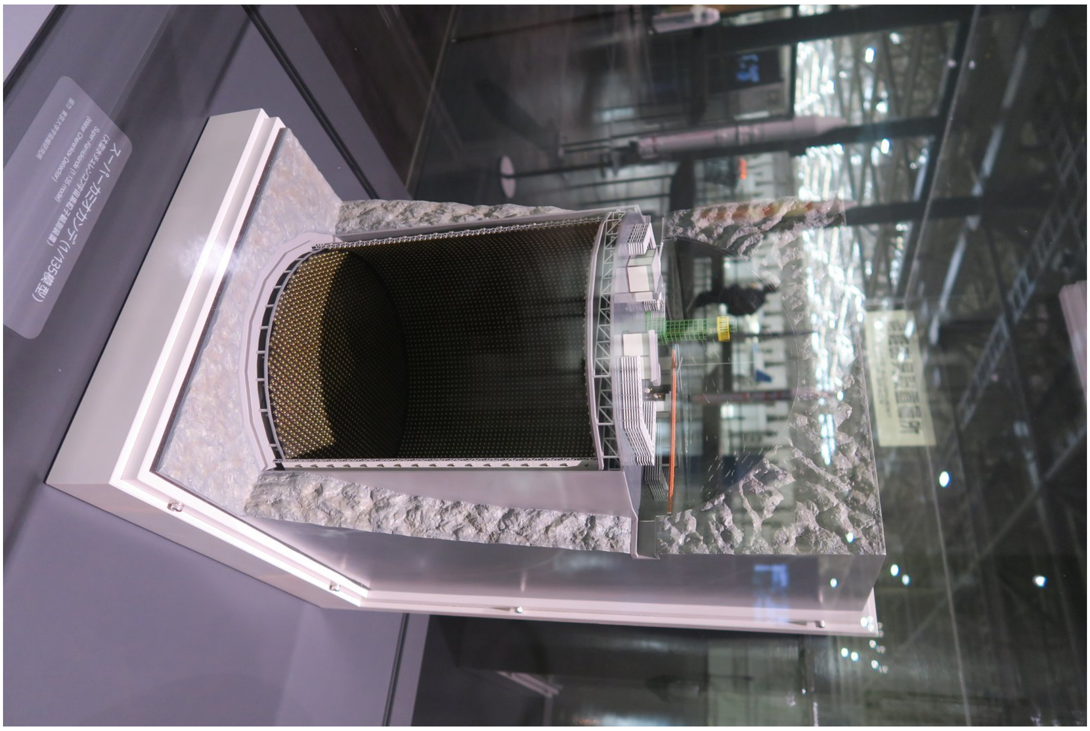

Figure 1.9: Interior of the Super-Kamiokande water Cherenkov detector (Kamioka, Japan), lined with photomultiplier tubes. Elastic scattering of solar neutrinos on electrons produces directional Cherenkov cones in such detectors. Image: Motohira (Wikimedia Commons), CC BY-SA 4.0.

deuterium it recorded three channels simultaneously:

$$\nu_e + d \to p + p + e^- \qquad \text{(charged current, } \nu_e \text{ only),} \tag{1.12}$$

$$\nu_x + d \to p + n + \nu_x \qquad \text{(neutral current, all active flavours),} \tag{1.13}$$

$$\nu_x + e^- \to \nu_x + e^- \qquad \text{(elastic scattering).} \tag{1.14}$$

The neutral-current flux matched Standard Solar Model expectations while the charged-current ν_e flux remained suppressed: the total active neutrino flux from ^{8}B fusion is correct, and a large fraction of ν_e have oscillated into other flavours before detection [1, 14]. Neutrino flavour change (vacuum oscillations plus Mikheyev–Smirnov–Wolfenstein matter effects in the solar density profile) therefore resolves the deficit without overturning the nuclear S-factors. Figure 1.10 shows the energy-dependent electron- neutrino survival probability for solar neutrinos, with day/night curves and the pp, ^{7}Be, pep, and ^{8}B measurement windows marked.

Key idea

- Lawson: $n\tau > 12k_BT/(\langle\sigma v\rangle Q)$ (DD estimate); triple product $n\tau T \gtrsim 3 \times 10^{21}\,\mathrm{m^{-3}\,keV\,s}$ for DT ballpark [1].
- Tokamak (JET, ITER): $\boldsymbol{B}_t + \boldsymbol{B}_p$ helices kill toroidal drifts [6].
- Inertial (NIF): huge n, tiny τ [6].
- Sun: weak pp clock + Gamow tunneling; neutrinos probe the core [1, 6].

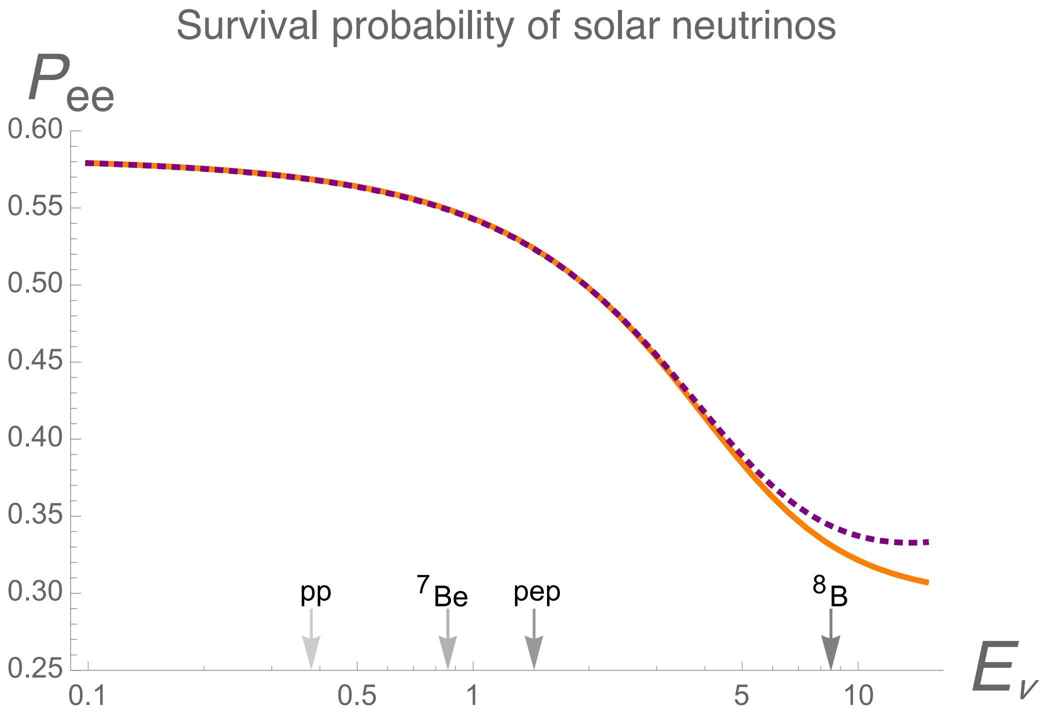

Figure 1.10: Electron-neutrino survival probability for solar neutrinos as a function of energy (day and night curves), with markers for *pp*, ^{7}Be, pep, and ^{8}B measurements. Adapted by F. Vissani from published oscillation analyses (Wikimedia Commons, CC BY-SA 4.0; after arXiv:1706.05435).

- Homestake $2.55 \pm 0.25\,\mathrm{SNU}$ vs $\sim 8\,\mathrm{SNU}$ predicted $\rightarrow$ flavour oscillation (SNO), not wrong S-factors [1].

1.7 Further physics from the literature

Bremsstrahlung floor. Electron–ion free–free radiation scales roughly as $n_e n_i Z_i^2 T^{1/2}$. Below a fuel-dependent temperature the radiation curve lies above the fusion power curve, so increasing density alone cannot ignite a pure plasma. High-Z wall impurities raise the floor sharply [6, 1].

Mirror and tandem-mirror concepts. Besides the tokamak torus, magnetic mirrors raise B at the ends of a linear device to reflect particles with large $v_\perp/v_\parallel$. Tandem-mirror and thermal-barrier variants are discussed in the standard surveys; they are less central to current reactor roadmaps than tokamaks and stellarators but illustrate the same cyclotron physics [6].

Tritium breeding. Neutron capture on lithium regenerates tritium,

$$^6\mathrm{Li} + n \rightarrow {}^4\mathrm{He} + {}^3\mathrm{H} + 4.8\,\mathrm{MeV}, \tag{1.15}$$

with an additional energetic channel on ^{7}Li [14, 1]. Without breeding, geological tritium cannot sustain a GW-scale $\mathrm{D} + \mathrm{T}$ economy.

MSW effect. Electron density in the Sun modifies effective neutrino masses (MSW). Adiabatic level crossing converts a large fraction of core ν_e into other active flavours before they reach

Earth, explaining ν_e-only deficits once the total flux is known [1, 14].

1.8 Problems with solutions

Problem 27.1 — Derive the Lawson inequality. Starting from $r = (n/2)^2\langle\sigma v\rangle$, $E_f = rQ\tau$, and $E_{\text{th}} = 3nk_BT$, derive $n\tau > 12k_BT/(\langle\sigma v\rangle Q)$. State every cancellation.

Solution 27.1.

$$E_f = \frac{n^2}{4}\langle\sigma v\rangle Q\tau, \qquad E_{\text{th}} = 3nk_BT.$$

Require $E_f > E_{\text{th}}$, cancel $n > 0$, and rearrange to (1.6) [1].

Problem 27.2 — Lawson scaling with reactivity. Explain why raising $\langle\sigma v\rangle$ at fixed T lowers the required $n\tau_E$. For $\mathrm{D+T}$ versus $\mathrm{D+D}$ at $k_BT = 10\,\text{keV}$, which fuel needs the larger confinement product?

Solution 27.2. $\langle\sigma v\rangle$ sits in the denominator of (1.6). At 10 keV, $\langle\sigma v\rangle_{\text{DT}}$ greatly exceeds the $\mathrm{D+D}$ value and radiation weighs more against $\mathrm{D+D}$, so $\mathrm{D+D}$ needs a much larger Lawson product [6, 1].

Problem 27.3 — Tokamak fields. Using the JET and ITER figures, explain why a purely toroidal magnetic field is insufficient and what role the plasma current plays in a tokamak.

Solution 27.3. Curvature/∇B drifts separate charges and drive $\boldsymbol{E}\times\boldsymbol{B}$ loss [6]. The plasma current supplies $\boldsymbol{B}_p$; together with $\boldsymbol{B}_t$ it twists field lines into closed helices so particles average over high- and low-B regions [6, 1].

Problem 27.4 — Inertial versus magnetic. Using Table 1.1 and the NIF chamber photograph, argue how inertial confinement can still satisfy Lawson despite $\tau \sim 10^{-11}\,\text{s}$.

Solution 27.4. Lawson constrains $n\tau$. With $n \sim 10^{31}\,\text{m}^{-3}$, even a $10^{-11}\,\text{s}$ disassembly time yields $n\tau \sim 10^{20}$ in SI units, comparable to a tokamak at $n \sim 10^{20}\,\text{m}^{-3}$ with $\tau \sim 1\,\text{s}$ [14, 6].

Problem 27.5 — Homestake threshold. Why did the Davis chlorine experiment miss most *pp* neutrinos? Which solar branches could it see? Quote the measured and predicted Homestake rates.

Solution 27.5. $E_{\text{th}} = 0.814\,\text{MeV}$ lies above the *pp* endpoint. Homestake sees mainly ^{8}B (with pep and ^{7}Be contributions). The values are $2.55 \pm 0.25\,\text{SNU}$ measured versus $8.0 \pm 1.0\,\text{SNU}$ predicted [1, 6].

Problem 27.6 — Neutrino versus photon information. Photons leave the photosphere; neutrinos leave the core. What does each messenger report?

Solution 27.6. Photons random-walk for 10^4–10^6 years and reflect transport-averaged surface conditions. Neutrinos free-stream from the core in minutes, so their spectrum probes nuclear burning rates today [6, 32].

Problem 27.7 — Why the deficit was not wrong S-factors. After SNO, how do we know the solar neutrino deficit was primarily a flavour effect? What does Fig. 1.10 add?

Solution 27.7. SNO's neutral-current channel counts all active flavours and matches Standard Solar Model fluxes, while ν_e-sensitive rates remain low: the total fusion rate is correct and ν_e have oscillated [1, 14]. The MSW survival curve shows that the suppression is energy dependent and consistent with matter-enhanced oscillation in the Sun.

Bibliography

[1] R. A. Dunlap, *An Introduction to the Physics of Nuclei and Particles* (2nd ed.), IOP Publishing, Bristol (2023), DOI: 10.1088/978-0-7503-6094-4, Ch. 3 (Nuclear composition and size).

[2] W. Demtröder, *Nuclear and Particle Physics*, Undergraduate Lecture Notes in Physics, Springer, Cham (2023).

[3] S. Petrera, *Problems and Solutions in Nuclear and Particle Physics*, UNITEXT for Physics, Springer, Cham (2019).

[4] F. Terranova, *A Modern Primer in Particle and Nuclear Physics*, Oxford University Press (2021).

[5] S. D'Auria, *Introduction to Nuclear and Particle Physics*, Undergraduate Lecture Notes in Physics, Springer, Cham (2018).

[6] K. S. Krane, *Introductory Nuclear Physics*, Wiley, New York (1988).

[7] R. Hofstadter, "Electron scattering and nuclear structure," Rev. Mod. Phys. **28**, 214 (1956).

[8] H. F. Ehrenberg, R. Hofstadter, U. Meyer-Berkhout, D. G. Ravenhall, and S. E. Sobottka, "High-Energy Electron Scattering and the Charge Distribution of Carbon-12 and Oxygen-16," Phys. Rev. **113**, 666 (1959).

[9] H. Yukawa, "On the interaction of elementary particles. I," Proc. Phys.-Math. Soc. Japan **17**, 48 (1935).

[10] R. D. Woods and D. S. Saxon, "Diffuse surface optical model for nucleon-nuclei scattering," Phys. Rev. **95**, 577 (1954).

[11] H. G. J. Moseley, "The high-frequency spectra of the elements," Phil. Mag. **26**, 1024 (1913); **27**, 703 (1914).

[12] C. F. von Weizsäcker, "Zur Theorie der Kernmassen," Z. Phys. **96**, 431 (1935).

[13] P. Cappellaro, *Introduction to Applied Nuclear Physics* (MIT OpenCourseWare / LibreTexts), CC BY-NC-SA 4.0.

[14] J.-L. Basdevant, J. Rich, and M. Spiro, *Fundamentals in Nuclear Physics: From Nuclear Structure to Cosmology*, Springer, New York (2005).

[15] D. Tong, *Particle Physics*, Lecture notes (University of Cambridge / CERN school notes).

[16] M. G. Mayer, "On closed shells in nuclei. II," Phys. Rev. **75**, 1969 (1949).

[17] O. Haxel, J. H. D. Jensen, and H. E. Suess, "On the "magic numbers" in nuclear structure," Phys. Rev. **75**, 1766 (1949).

[18] T. Schmidt, "Über die magnetischen Momente der Atomkerne," Z. Phys. **106**, 358 (1937).

[19] L. W. Nordheim, "On spins, moments, and shells in nuclei," Phys. Rev. **78**, 294 (1950).

[20] Evaluated Nuclear Structure Data File (ENSDF), National Nuclear Data Center, Brookhaven National Laboratory, `https://www.nndc.bnl.gov/ensdf/`.

[21] NuDat 3, National Nuclear Data Center, Brookhaven National Laboratory, `https://www.nndc.bnl.gov/nudat3/`.

[22] N. J. Stone, "Table of nuclear magnetic dipole and electric quadrupole moments," At. Data Nucl. Data Tables **90**, 75 (2005); updated compilations at NNDC.

[23] W. N. Cottingham and D. A. Greenwood, *An Introduction to Nuclear Physics* (2nd ed.), Cambridge University Press, Cambridge (2001).

[24] H. Geiger and J. M. Nuttall, "The ranges of the α particles from the radioactive substances," Phil. Mag. **22**, 613 (1911).

[25] G. Gamow, "Zur Quantentheorie des Atomkernes," Z. Phys. **51**, 204 (1928).

[26] R. W. Gurney and E. U. Condon, "Wave mechanics and radioactive disintegration," Nature **122**, 439 (1928); Phys. Rev. **33**, 127 (1929).

[27] M. Wang, W. J. Huang, F. G. Kondev, G. Audi, and S. Naimi, "The AME 2020 atomic mass evaluation (II). Tables, graphs and references," Chin. Phys. C **45**, 030003 (2021).

[28] Laboratoire National Henri Becquerel (LNHB), Recommended decay data, `http://www.lnhb.fr/nuclear-data/nuclear-data-table/`.

[29] L. M. Langer, R. D. Moffat, and H. C. Price, Jr., "Low energy beta-ray spectra: P^{32} and Cu^{64}," Phys. Rev. **76**, 1725 (1949).

[30] L. M. Langer and H. C. Price, Jr., "Shapes of the beta-spectra of the forbidden transitions of Sb^{124}, Rb^{86}, Sr^{89}, Y^{91}, and Cs^{137}," Phys. Rev. **75**, 1769 (1949).

[31] D. C. Camp and L. M. Langer, "The shape of the ^{66}Ga positron spectrum and the contribution from $0^+ \to 0^+$ transitions," Phys. Rev. **129**, 1782 (1963).

[32] H. C. Verma, *Nuclear Physics: Fundamentals and Applications*, NPTEL/IIT Kanpur lecture series, `https://hcverma.in/ncl_phy_lectures`.

[33] International Atomic Energy Agency, *LiveChart of Nuclides*, evaluated structure, decay, reaction, and fission-yield data, `https://www-nds.iaea.org/relnsd/vcharthtml/VChartHTML.html`.

[34] T. Kibédi, T. W. Burrows, M. B. Trzhaskovskaya, P. M. Davidson, and C. W. Nestor, Jr., "Evaluation of theoretical conversion coefficients using BrIcc," Nucl. Instrum. Methods Phys. Res. A **589**, 202 (2008), DOI: 10.1016/j.nima.2008.02.051.

[35] D. A. Brown *et al.*, "ENDF/B-VIII.0: The 8th major release of the nuclear reaction data library with CIELO-project cross sections, new standards and thermal scattering data," Nucl. Data Sheets **148**, 1 (2018), DOI: 10.1016/j.nds.2018.02.001.

[36] B. Acharya *et al.*, "Solar fusion III: New data and theory for hydrogen-burning stars," Rev. Mod. Phys. **97**, 035002 (2025), DOI: 10.1103/8lm7-gs18.

[37] E. M. Burbidge, G. R. Burbidge, W. A. Fowler, and F. Hoyle, "Synthesis of the elements in stars," Rev. Mod. Phys. **29**, 547 (1957), DOI: 10.1103/RevModPhys.29.547.

[38] F. Hoyle, "On Nuclear Reactions Occurring in Very Hot Stars. I. The Synthesis of Elements from Carbon to Nickel," Astrophys. J. Suppl. **1**, 121 (1954), DOI: 10.1086/190005.

[39] S. N. Ghoshal, "An experimental verification of the theory of compound nucleus," Phys. Rev. **80**, 939 (1950), DOI: 10.1103/PhysRev.80.939.

[40] D. Adhikari *et al.* (PREX Collaboration), "Accurate determination of the neutron skin thickness of ^{208}Pb through parity-violation in electron scattering," Phys. Rev. Lett. **126**, 172502 (2021), DOI: 10.1103/PhysRevLett.126.172502.

[41] B. T. Reed, F. J. Fattoyev, C. J. Horowitz, and J. Piekarewicz, "Implications of PREX-II on the equation of state of neutron-rich matter," Phys. Rev. Lett. **126**, 172503 (2021), DOI: 10.1103/PhysRevLett.126.172503.

[42] B. Hu *et al.*, "Ab initio predictions link the neutron skin of ^{208}Pb to nuclear forces," Nature Phys. **18**, 1196 (2022), DOI: 10.1038/s41567-022-01715-8.

[43] E. Epelbaum, H.-W. Hammer, and U.-G. Meißner, "Modern theory of nuclear forces," Rev. Mod. Phys. **81**, 1773 (2009), DOI: 10.1103/RevModPhys.81.1773.

[44] H.-W. Hammer, S. König, and U. van Kolck, "Nuclear effective field theory: Status and perspectives," Rev. Mod. Phys. **92**, 025004 (2020), DOI: 10.1103/RevModPhys.92.025004.

[45] T. Otsuka, A. Gade, O. Sorlin, T. Suzuki, and Y. Utsuno, "Evolution of shell structure in exotic nuclei," Rev. Mod. Phys. **92**, 015002 (2020), DOI: 10.1103/RevModPhys.92.015002.

[46] H. Hergert, S. K. Bogner, T. D. Morris, A. Schwenk, and K. Tsukiyama, "The in-medium similarity renormalization group: A novel ab initio method for nuclei," Phys. Rep. **621**, 165 (2016), DOI: 10.1016/j.physrep.2015.12.007.

[47] J. M. Lattimer and M. Prakash, "The equation of state of hot, dense matter and neutron stars," Phys. Rep. **621**, 127 (2016), DOI: 10.1016/j.physrep.2015.12.005.

[48] J. M. Lattimer, "Neutron stars and the nuclear matter equation of state," Annu. Rev. Nucl. Part. Sci. **71**, 433 (2021), DOI: 10.1146/annurev-nucl-102419-124827.

[49] B. P. Abbott *et al.* (LIGO Scientific Collaboration and Virgo Collaboration), "GW170817: Observation of gravitational waves from a binary neutron star inspiral," Phys. Rev. Lett. **119**, 161101 (2017), DOI: 10.1103/PhysRevLett.119.161101.

[50] M. J. Dolinski, A. W. P. Poon, and W. Rodejohann, "Neutrinoless double-beta decay: Status and prospects," Annu. Rev. Nucl. Part. Sci. **69**, 219 (2019), DOI: 10.1146/annurev-nucl-101918-023407.

[51] M. Agostini, G. Benato, J. A. Detwiler, J. Menéndez, and F. Vissani, "Toward the discovery of matter creation with neutrinoless $\beta\beta$ decay," Rev. Mod. Phys. **95**, 025002 (2023), DOI: 10.1103/RevModPhys.95.025002.

[52] P. Gysbers *et al.*, "Discrepancy between experimental and theoretical β-decay rates resolved from first principles," Nature Phys. **15**, 428 (2019), DOI: 10.1038/s41567-019-0450-7.

[53] H. L. Crawford, K. Fossez, S. König, and A. Spyrou, "A vision for the science of rare isotopes," Annu. Rev. Nucl. Part. Sci. **74**, 141 (2024), DOI: 10.1146/annurev-nucl-121423-091501.

[54] Nuclear Science Advisory Committee, *A New Era of Discovery: The 2023 Long Range Plan for Nuclear Science*, U.S. Department of Energy and National Science Foundation (2023), `https://nuclearsciencefuture.org/`.

[55] S. A. Giuliani, Z. Matheson, W. Nazarewicz, E. Olsen, P.-G. Reinhard, J. Sadhukhan, B. Schuetrumpf, N. Schunck, and P. Schwerdtfeger, "Colloquium: Superheavy elements: Oganesson and beyond," Rev. Mod. Phys. **91**, 011001 (2019), DOI: 10.1103/RevModPhys.91.011001.

[56] N. Schunck and D. Regnier, "Theory of nuclear fission," Prog. Part. Nucl. Phys. **125**, 103963 (2022), DOI: 10.1016/j.ppnp.2022.103963.

[57] I. Counts, J. Hur, D. P. L. Aude Craik, H. Jeon, C. Leung, J. C. Berengut, A. Geddes, A. Kawasaki, W. Jhe, and V. Vuletić, "Evidence for nonlinear isotope shift in Yb^+ search for new boson," Phys. Rev. Lett. **125**, 123002 (2020), DOI: 10.1103/PhysRevLett.125.123002.

[58] I. Angeli and K. P. Marinova, "Table of experimental nuclear ground state charge radii: An update," At. Data Nucl. Data Tables **99**, 69 (2013), DOI: 10.1016/j.adt.2011.12.006.

[59] S. Kraemer *et al.*, "Observation of the radiative decay of the ^{229}Th nuclear clock isomer," Nature **617**, 706 (2023), DOI: 10.1038/s41586-023-05894-z.